Tribological properties of Mullite/3Y-TZP ceramics with different content of mullite fabricated by gel-casting

Huang, Yan qi; Li, Zhuan; Liu, Peng fei; Huang, Tian xing; Li, Yang; Xiao, Peng

Published in:
Applied Surface Science

DOI (link to publication from Publisher):
10.1016/j.apsusc.2018.12.291

Publication date:
2019

Document Version
Accepted author manuscript, peer reviewed version

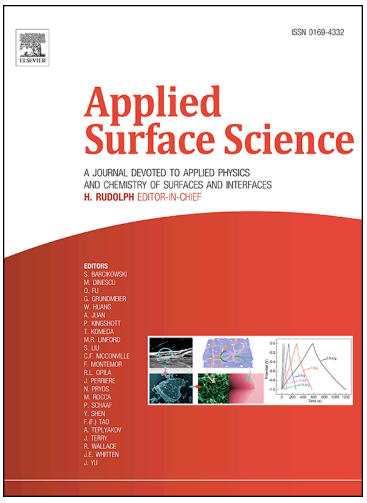

Full Length Article

Tribological properties of Mullite/3Y-TZP ceramics with different content of mullite fabricated by gel-casting

Yan-qi Huang, Zhuan Li, Peng-fei Liu, Tian-xing Huang, Yang Li, Peng Xiao

PII: S0169-4332(18)33638-9
DOI: https://doi.org/10.1016/j.apsusc.2018.12.291
Reference: APSUSC 41388

To appear in: *Applied Surface Science*

Received Date: 30 October 2018
Revised Date: 27 December 2018
Accepted Date: 31 December 2018

Please cite this article as: Y-q. Huang, Z. Li, P-f. Liu, T-x. Huang, Y. Li, P. Xiao, Tribological properties of Mullite/3Y-TZP ceramics with different content of mullite fabricated by gel-casting, *Applied Surface Science* (2018), doi: https://doi.org/10.1016/j.apsusc.2018.12.291

Tribological properties of Mullite/3Y-TZP ceramics with different content of mullite fabricated by gel-casting

Yan-qi Huang[b], Zhuan Li[a,b*], Peng-fei Liu[c], Tian-xing Huang[b], Yang Li[a,b], Peng Xiao[a,b*]

[a]*National Key Laboratory of Science and Technology for National Defence on High-strength Structural Materials, Central South University, Changsha 410083,China*

[b]*State Key Laboratory of Powder Metallurgy, Central South University, Changsha 410083, PR China*

[c]*Department of Chemistry and Bioscience, Aalborg University, Fredrik Bajers Vej 7H, 9220 Aalborg, Denmark*

Abstract: In-situ mullite toughened 3Y-TZP ceramics (Mullite/3Y-TZP ceramics) with different content of mullite were prepared by gel-casting combined with pressureless sintering to study effects of the content of mullite on their microstructure and tribological properties. The results indicated that the mullite uniformly distributed in the zirconia matrix had a complete columnar structure and a moderate content in S2 (the sample containing 4mol% mullite), and the smooth surface caused by low porosity combined with the good mechanical properties significantly reduced the coefficient of friction and wear rate of S2. A high proportion of irregular mullite destroyed the overall structure of S3-S5 (the samples containing 6, 8 and 10mol% mullite, respectively), combined with high porosity not only reduced the mechanical properties of them, but also led to an increment in surface roughness, which

* Corresponding authors at: National Key Laboratory of Science and Technology for National Defence on High-strength Structural Materials, Central South University, Changsha 410083, China.

Email addresses: lizhuan@csu.edu.cn (Z. Li); xiaopeng@csu.edu.cn (P. Xiao)

significantly lowered the wear resistance of the material. Studies of worn surfaces showed that micro-cutting was present in every sample, but the degree of micro-cutting and adhesive wear in S2 were minimal due to its good structure and properties. However, the micro-cutting and adhesive wear of S3-S5 were exacerbated.

Key words: Mullite/3Y-TZP ceramics; Tribological properties; Microstructure; Wear rate; Wear mechanisms

1. Introduction

Wear and corrosion are two of the main reasons why materials fail during engineering applications, especially when the parts are subject to joint attack by both [1]. As an oxide ceramic, 3Y-ZrO_2 ceramic has attracted much attention in the mechanical and biological fields due to its good mechanical properties, corrosion resistance and biocompatibility, being expected as a promising wear-resistant material applied in harsh environments [2-4]. However, although the presence of Y_2O_3 stabilizer reduces the volume change caused by phase transitions in 3Y-ZrO_2 ceramic, it tends to fail due to the inherent brittleness under the stresses caused by thermal shock, erosion and wear processes [5,6]. Moreover, the brittleness caused by low fracture toughness not only makes it brittle in practical applications, but also causes large wear due to spalling during the process of friction. Considering that the high requirements for its tribological properties in both biological and mechanical fields, it is necessary to reduce the wear rate based on the improvement of toughness. In order to solve this problem, a large number of studies have shown that the addition of second phase particles are considered to be the most promising method [7-9].

At present, a series of measures have been used to improve 3Y-ZrO_2 ceramic, such as

the addition of second phase particles which include whiskers, particles and platelets with excellent properties [10,11]. However, although these measures have improved brittleness to some extent, they all have their own disadvantages, such as thermal mismatch with the matrix, oxidation at high temperatures and uneven distribution in the matrix [11,12]. Mullite ($3Al_2O_3 \cdot 2SiO_2$) is the only stable silico-aluminate in the binary system of SiO_2-Al_2O_3 at atmospheric pressure which does not react with the matrix [13-15]. It has broad prospects in the field of reinforcing materials for ceramic matrix composites by preventing the spread of microcracks due to its high strength, low coefficient of thermal expansion and thermal conductivity, excellent corrosion resistance and oxidation resistance [16-22].

Meanwhile, currently extensive research has been conducted on the field of tribology involved in practical applications of zirconia ceramics. Previous research work has shown that the tribological properties of 3Y-ZrO_2 ceramic are affected by the content of second phase particles (Al_2O_3) [23]. The result indicated that the ceramic had excellent tribological properties when 10wt% Al_2O_3 was added, because they had lower surface roughness and optimum mechanical properties, including higher hardness and fracture toughness. The effect of heat treatment on the tribological properties of 3Y-ZrO_2 ceramic was also studied [24]. It was found that the wear behavior of the samples after two different heat treatments was about the same at low speed, but the material with fine grain structure had higher wear resistance at high speed. The increment of wear rate in the material may be caused by the phase transformation due to the existence of compressive stress, which led to the change of

volume and the generation of cracks, thereby causing grain to fall off.

However, in view of few reports on the tribological properties of Mullite/3Y-TZP composite ceramics, this study will be based on the existing research including the study of the microstructure and mechanical properties of Mullite/3Y-TZP composite ceramics, using in-situ mullite combine with gel-casting process to prepare the composite ceramics, and further study the influence of the content of mullite on the tribological properties of it and explore its optimal composition, which provides a theoretical basis for its application [25].

2. Experimental procedure

2.1. Preparation of Mullite/3Y-TZP composite ceramics

The specific preparation process of Mullite/3Y-TZP composite ceramics is described as follows: Firstly, the premixed solution which consist of monomer, dispersant and cross-linking agent was mixed with raw material powder, and then the obtained mixture was milled for 4h to obtain slurry; Secondly, the catalyst and the initiator were added dropwise to the slurry placed in nitrogen atmosphere while being stirred, and then poured it into a mold to obtain a green body; Thirdly, the green body was subjected to liquid phase drying and air drying; Finally, the product was obtained by sintering the dried object. More details about the experimental process and the raw materials used in this study were described in the literature of Liu et al [26].

2.2. Characterization methods

The open porosity of the samples was measured by the Archimedes method in distilled water, and the accuracy of electronic balance was 0.0001g. Five pieces of

samples were used to measure the open porosity at each kind of sample. The computational formula is as follows:

$$P = \frac{m_1 - m_2}{m_3} \times 100\% \quad (1)$$

Where m_1 represents the total mass measured after the pores of the sample are filled with water; m_2 represents the actual mass of the sample; m_3 represents the reading of the electronic scale obtained by suspending the sample in distilled water, that is, the mass of the discharged water; P stands for open porosity of the sample.

The microstructure of the samples and the morphology of worn surfaces after rubbing were observed by Scanning electron microscope (SEM, JSM-6390, JEOL, Tokyo, Japan). Before SEM analysis, the surface of the samples was washed and dried, then a thin layer of Au film was coated on the surface of the sample by spraying gold for 120s, so as to achieve higher resolution of surface scanning. Using X-ray diffraction (XRD, Cu Ka radiation, D/max-2550-18kW, Rigaku, Japan) from 15° to 70° at 40kV with a scanning speed of 8°/min to analyze the composition and state of phases in zirconia matrix. The distribution of various elements and phases was investigated by electron probe microanalysis (EPMA, JEOL CO, Jxa-8230). Laser scanning confocal microscope (LSM700, Zeiss Axio, German) was used to characterize the three-dimensional (3D) morphology of the worn surfaces in the samples.

2.3. Tribological tests

All the tribological tests were carried out on the MMD-1 Multifunctional Friction and Wear Tester. The actual picture and schematic diagram of the friction experiment were shown in **Fig. 1**. The discoidal high-chromium cast iron (Cr_{26}) with the dimension of

Φ45mm×4mm was used as the mated ring because it had a high hardness that matched the ceramic, and the tribological tests was carried out in the oil environment using the pin-disc friction method in the context of its application in the mechanical field. Various performance parameters of the mated ring and oil were shown in **Table 1**. The dimensions of the cylindrical samples for tribological tests were Φ4mm× 10mm. Each set of samples and mated rings were polished prior to rubbing. In order to obtain the wear trace and analyze the wear mechanism of the sample on the basis of it, large load and high sliding velocity were adopted. Different samples were rubbed at 200r/min for 30 min in oil environment with an applied load of 150N and the room temperature was kept constant during this period. The setting of various parameters during the friction process was shown in **Table 2**. The frictional testing machine will automatically collect the friction coefficient curve during the friction process. After the rubbing process, the rubbed sample was ultrasonically cleaned and dried, and then the wear rate was calculated by mass loss. Finally, 3D morphology of the worn surface was characterized by LSM700 to determine the width and depth of the worn track. The wear mechanism was studied by analyzing the SEM topography of the worn surface.

3. Results and discussion

3.1 X-Ray and microstructural analysis

XRD pattern in **Fig. 2** shows that besides the existence of main crystalline phases (m-ZrO_2, C-ZrO_2 and t-ZrO_2), the diffraction peaks of mullite and Al_2O_3 begin to appear when the content of mullite increases to 4mol%. This phenomenon indicates

that there is almost no mullite in S1, but an appropriate amount of mullite has been formed in S2, and there are Al_2O_3 particles which are not involved in reaction as well. With the increase of the content of mullite (S3-S5), the intensity of diffraction peaks of the three materials increases obviously, which indicates that their crystallinity has increased and obvious growth has taken place. And their existence and content have an important influence on the microstructure and mechanical properties of the samples.

In the previous work, the microstructure of various samples with different content of mullite has been systematically described [25]. In view of the relatively large difference between 2, 4 and 10mol%, we select S1, S2 and S5 as the research objects to further study the influence of different microstructure on the tribological properties. **Fig. 3(a-c)** represents the surface microtopography of three different samples (S1, S2 and S5), each of which was polished prior to testing. The black part is mullite and the off-white part is zirconia [25]. As shown in **Fig. 3(a)**, zirconia particles in S1 are tightly coated around a small amount of columnar mullite generated by reaction, and the two are tightly bonded. Zirconia particles have a small particle size and are closely connected to each other. In this sample, the porosity is low and the pore size is small, making the surface smoother [27]. And combined with the higher mechanical properties of S1 due to the strong intergranular bonding and low porosity, the coefficient of friction and wear rate are reduced[28]. At the same time, the sample with fine-grained zirconia structure also has good wear resistance under high-speed sliding [24]. Compared with S1, it can be observed from **Fig. 3(b)** that columnar

mullite grows significantly while the content increases in S2. The columnar mullite uniformly distributed on the zirconia matrix is closely connected to the fine zirconia particles which do not undergo a large amount of aggregation. In addition, according to the XRD and EPMA analysis, the sample also contains unreacted alumina particles, and the strengthening and toughening effect of the presence of alumina particles and columnar mullite significantly improves the mechanical properties of the material [25,26]. Good comprehensive mechanical properties combined with extremely low porosity make it difficult for materials to undergo large brittle fracture and shedding during friction, thus improving the wear resistance of the material [23,27,28]. However, great changes have taken place in the microstructure of S5, as shown in **Fig. 3(c)**. In addition to the previously described and analyzed the phenomenon that mullite is in the form of particles or fluids and are connected to each other, it has also been found that zirconia particles are agglomerated and even exposed on the surface of the sample; more pores are produced and the pore size becomes larger. All of these phenomena indicate that the bonding force between the particles is weak and the surface of the sample becomes rough, which will significantly affect the tribological properties of the material.

Taking S2 as an example, the distribution of different phases and elements inside is further clarified in the EPMA diagram, as shown in **Fig. 4(a-f)**. It can be seen from **Fig. 4(a)** that a large amount of columnar mullite is formed in the sample, and it is uniformly distributed in the zirconia matrix. **Fig. 4(b)** and **(f)** show that zirconia particles are uniformly distributed in the mullite besides being distributed around the

columnar mullite, which can also be demonstrated in **Fig. 3(a)**. This is consistent with the previous SEM analysis, and it can be used to explain the effect of zirconia particles embedded in mullite on the mechanical properties of mullite [25]. In addition, besides the columnar mullite being black in **Fig. 4(a)**, there are many black spots. Combined with the XRD and the distribution of aluminum elements in **Fig.4(c)**, it can be determined that the black spots are residual Al_2O_3 particles, which proves that Al_2O_3 particles do not fully react to form mullite. And the pinning effect of residual alumina particles will play an important influence on the mechanical properties of ceramics, which would further affect the tribological properties. **Fig. 4(d)** shows the distribution of Si elements. In addition to the high content of Si elements in mullite, Si elements are also widely present in areas other than mullite. This is because of the fluidity of the liquid phase in the Y_2O_3-SiO_2-Al_2O_3 ternary system, SiO_2 particles that do not participate in the reaction to form mullite formed a glass phase after sintering, and is widely present in the matrix [29-31]. As can be clearly seen from **Fig. 4(e)**, Y element is distributed inside the zirconia matrix uniformly. It is shown that Y has been incorporated into the zirconia lattice, which effectively stabilizes the tetragonal/cubic zirconia phase. In addition, Y element also aggregates near the mullite, which promotes the formation of a columnar mullite phase, thereby improving the mechanical properties [26].

3.2 *Tribological behavior*

The curves of the coefficient of friction for all the different samples are shown in **Fig.5**. although their variation trends are roughly the same, the values of the friction

coefficients are obviously different. The purple curve represents the change of the friction coefficient of S2. It can be seen that the curve is the lowest, indicating that the friction coefficient of S2 is the smallest, only reaches 0.098, which is closely related to its dense and intact structure produced by uniform distribution of columnar mullite and good mechanical properties, as shown in **Table 3**. It can be seen that S2 retains a high hardness value, and comparative analysis shows that the comprehensive mechanical properties of S2 are optimal among the tested samples. Compared with S2, the friction coefficients of S1 and S3 increase slightly because of the decreased mechanical properties of the samples caused by the content and structure of mullite, as shown in the green and black curves. Although the microstructure of S1 is not as perfect as that of S2, its dense structure and the uniform distribution of a small amount of columnar mullite also make it very hard and have higher fracture toughness and bending strength than that of S3, so the friction coefficient of S1 is lower than that of S3. The fluid-shaped irregular mullite in S4 and S5 is difficult to strengthen the zirconia matrix, and their existence alters the overall structure of the composite ceramics. Therefore, they not only reduce the overall hardness of the sample, but also make other mechanical properties very poor [25]. In addition, the resulting non-dense structure increases surface roughness. Therefore, it is not difficult to conclude that their friction coefficients are relatively large, as shown in the red and blue curves in the figure.

Fig. 6 shows the change of wear rate of different samples after 30min of rubbing under 150N load. It is intuitive to note that there is a corresponding relationship

between friction coefficients and wear rate. Obviously, the wear rate of the samples decreases first and then increases with the increase of the content of mullite, and the minimum value appears when the content of mullite reaches 4mol% (S2), which is about 3.2×10^{-4}. The wear rate of S1 is significantly higher than that of S2, which indicates that high hardness alone is not enough to reduce the wear rate. It is further noted when the content of mullite exceeds 4mol%, the samples begin to shift from slight wear to severe wear, and the wear rate in S5 has increased to 1.7×10^{-3}, about 5 times that of S2. The increment of wear rate is because of the fact that the particles on the worn surface are spalled during the friction process due to the decrease in the mechanical properties and the increased porosity of the samples.

To investigate the undulation of the surface and the depth of the grooves after rubbing, three dimensional (3D) morphology of the worn surface of five different samples has been characterized respectively, as shown in **Fig. 7(a-e)**. The morphology of the worn surface of S1 is shown in **Fig. 7(a)**. The blue part on the left represents a relatively flat surface with a small number of grooves and a shallow depth; the yellow part indicates a large surface undulation. The curve below the graph represents the undulation of the worn surface. It can be seen from the curve that the depth of grooves on the surface is different, indicating that the friction of the sample is not uniform, which may be caused by the uneven force of the friction, or the difference in the mechanical properties of the sample itself. The curve shows that the depth of the grooves in most areas is shallow, but it even reaches 12-15μm in some places, and the grooves are found to be wider in the right area. This is why the wear rate of S1 is high.

The 3D microscopic morphology of the worn surface of S2 is shown in **Fig. 7(b)**. It is obvious that the uniformity of the color indicates that the worn surface is uniform, which is closely related to the uniform force of S2 during the friction process and its good microstructure and mechanical properties. The curve below the graph shows that the grooves on the worn surface are very shallow and only reach 8-10μm in some places, which confirm that the friction coefficient and wear rate of S2 are small. In **Fig. 7(c)**, it can be seen that the microscopic morphology of S3 has changed significantly. Although the worn surface is uniformly distributed, the average depth increases significantly and the depth in the local area is even 12-14μm, which indicate a significant increment in the wear rate of the sample. The peaks on the curves in **Fig.7(d)** and **(e)** became denser, and the changes between the peaks and valley are relatively large, indicating that the number and depth of grooves had increased. These all confirm that the friction coefficient and wear rate of S4 and S5 increase with the roughness of the worn surface.

3.3 Wear mechanism

The morphologies of worn surface offer clues to the wear mechanisms involved in sliding wear of the samples. **Fig. 8(a)** represents the morphology of worn surface of S1 after being rubbed for 30min under a 150N load. Scratches and grooves parallel to the sliding direction are clearly visible in the micrograph. The main reason for the formation of the wavy pattern of these grooves is the plowing effect of hard debris which are mainly produced by the flaking of zirconia or mullite particles on the worn surface due to thermal stress caused by an increase in temperature and compressive

stress during friction. At the same time, high hardness and low fracture toughness make it difficult for the sample to undergo plastic deformation, and on the contrary, it is easy for large fragments to fall off, which is the reason why there are large pits in the figure. The surface morphology of S2 with fine grain structure is very flat outside the hole after rubbing, as shown in **Fig. 8(b)**. The obvious difference from S1 is that the grooves are very shallow and few. The main reason for this phenomenon is the good overall mechanical properties produced by the good microstructure of S2, which significantly improve its tribological properties. These good mechanical properties are caused by the pinning effect of the uniform distribution of columnar mullite and residual alumina in the matrix [25]. In addition, it can be seen that there are few large pores on the worn surface, indicating that no large particles are peeled off during the rubbing process and only mild abrasive wear occurs, which are the reason why the deep grooves do not occur in Fig. 7(b). As shown in **Fig. 8(c-e)**, unlike the phenomenon described in S1, the number and depth of grooves and scratches parallel to the rubbing direction of the sample increase as the content of mullite increases, indicating that the irregular shape of mullite does not make the tribological properties of these samples higher than that of S2, but reduces the wear resistance of the materials due to the lower mechanical properties. Due to the relatively rough surface of the S3-S5 sample, the higher porosity allows the new zirconia particles to be re-exposed to the surface during the rubbing process, while the relatively loose structure reduces the connection between the particles, resulting in increased shedding of debris during friction. Therefore, more serious abrasive wear occurs on the surface

of the sample. In addition, due to the decrease in hardness and strength of the sample, the deformation of the sample during the rubbing process is easier than that of S1 and 2. It can be seen from the figure that some of their regions are plastically deformed.

Fig. 9(a) is a further enlargement of the worn surface of sample S1. It can be seen that there are indeed pits caused by brittle fracture, and there are also many microcracks which may be due to phase changes that occur under stress. This further proves that particle shedding occurs during the friction process, resulting in micro-cutting of the sample, which belongs to abrasive wear. In this case, the wear mechanism is shown in **Fig. 10(a)** and **(b)**. In the friction process, the actual contact area is far less than the apparent contact area due to the difference in surface height between the sample and the mated ring on the macro level and the roughness caused by the arrangement of grains on the surface of the sample on the micro level. The rigid particles protruding from the surface of the sample contact with the matching ring, and are detached due to the pressure during the sliding process. The abrasive chips existing between the friction surfaces are partially embedded in the sample and the mating ring under the action of the pressing force, and the furrows are generated on the surface of the sample during the further sliding, which is called abrasive wear. The presence of adhesive layered material on the worn surface indicates that slight adhesive wear occurs on S2, as shown in **Fig. 9(b)**. The main reason can be explained by **Fig. 10(a)** and **(c)**. The surface of S2 is relatively smooth, which increases its contact area with the mating ring. Under the conditions of high load and high speed sliding, the instantaneous high temperature causes Cr_{26} to soften and make the two bonding

surfaces adhere to each other, resulting in the migration of materials. However, due to the high mechanical properties of the two and the presence of the lubricating oil film, the surfaces of the sample do not tear or even fell off a large area, but only slight adhesive wear occurs. Compared with **Fig. 9(a-b)**, the plastic deformation regions of S3-S5 increase under the action of compressive stress, and the plastic flow of the material in the sliding direction causes the formation of cavities, as shown in **Fig. 9(c)**. This indicates that these samples have a more severe adhesive wear and abrasive wear during the rubbing process. Although lubricants can enter the cavity during friction to reduce frictional resistance, their wear rate is still higher than S2. Therefore, the wear rate of these samples is significantly increased. Its wear mechanism can also be described in **Fig.10(a-c)**.

4. Conclusions

Mullite/3Y-TZP composite ceramics were prepared by gel-casting combine with pressureless sintering. The effects of different content of mullite on the microstructure and tribological properties of Mullite/3Y-TZP composite ceramics were studied. The main results can be summarized as follows:

(1) The microstructure of S2 is excellent. Complete columnar mullite and residual alumina particles uniformly distributed in the matrix improve the mechanical properties of the material. The dense structure resulting from low open porosity increases the bonding force between different particles, which not only improves the performance, but also makes the sample surface smoother.

(2) The wear resistance of S2 is excellent owing to its good microstructure and

mechanical properties. It has a lower friction coefficient and wear rate than other samples. Although S1 has a high hardness, its fracture toughness and flexural strength are low, so that the tribological properties are not as good as those of the S2. S3, S4 and S5 have poor tribological properties due to their poor structure and overall mechanical properties.

(3) Each sample undergoes micro-cutting during the rubbing process. In addition, slight adhesive wear also occurs in S2 while it exacerbates in S3-S5. High hardness and good bond strength between grains only cause slight wear in S2, but S3-S5 is easy to deform and fall off during friction due to lower hardness and poor mechanical properties, resulting in heavy abrasive wear and adhesive wear.

Acknowledgements

The authors would like to thank the National Natural Science Foundation of China (Grant No. 51575536) and the State Key Laboratory of Powder Metallurgy for their financial support.

References

[1] N. Chawla, K. K. Chawla, Wear and corrosion, Metal Matrix Composites. 95 (2013) 261-271.

[2] X. Q. Cao, R. Vassen, D. Stoever, Ceramic materials for thermal barrier coatings, J. Eur. Ceram. Soc. 24 (2004) 1-10.

[3] S. F. Hulbert, F. A. Young, R. S. Mathews, Potential of ceramic materials as permanently implantable skeletal prostheses, J. Biomed. Mate. Res. A. 4 (1970) 433-456.

[4] A. G. Evans, Perspective on the development of high-toughness ceramics, J. Am. Ceram. Soc. 72 (1990) 187-192.

[5] P. F. Becher, Toughening behavior in ceramics associated with the transformation of tetragonal ZrO_2, Acta. Metall. 34 (1986) 1885-1891.

[6] E. Medvedovski, R. J. Liewellyn, Oxide ceramics for abrasion and erosion resistance applications, Ceram. Int. 51 (2002) 120-126.

[7] S. Ran, L. Winnubst, D. H. A. Blank, Effect of microstructure on the tribological and mechanical properties of CuO-Doped 3Y-TZP ceramics, J. Am. Ceram. Soc. 90 (2010) 2747-2752.

[8] J. Sun, L. Gao, M. Iwasa, T. Nakayama, K. Niihara, Failure investigation of carbon nanotube/3Y-TZP nanocomposites, Ceram. Int. 31 (2005) 1131-1134.

[9] F. Inam, H. Yan, M. J. Reece, T. Peijs, Structural and chemical stability of multiwall carbon nanotubes in sintered ceramic nanocomposite, Adv. Appl. Ceram. 109 (2010) 240-247.

[10] C. Ionascua, R. Schaller, High temperature mechanical loss spectrum of 3Y-TZP zirconia reinforced with carbon nanotubes or silicon carbide whiskers, Solid State Phenom. 137 (2008) 29-34.

[11] J. Hong, L. Gao, B. A. Shaw, D. P. Thompson, SiC platelet and SiC platelet - alumina reinforced TZP matrix composites, Br. Ceram. Trans. 94 (1995) 201-204.

[12] F. Inam, H. Yan, M. J. Reece, T. Peijs, Structural and chemical stability of multiwall carbon nanotubes in sintered ceramic nanocomposite, Adv. Appl. Ceram. 109 (2010) 240-247.

[13] H. Schneider, J. Schreuer, B. Hildmann, Structure and properties of mullite-A review, J. Eur. Ceram. Soc. 28 (2008) 329-344.

[14] R. E. Ouatib, S. Guillemet, B. Durand, A. Samdi, L. E. Rakho, R. Moussa, Reactivity of aluminum sulfate and silica inmolten alkali-metal sulfates in order to prepare mullite, J. Eur. Ceram. Soc. 25 (2005) 73-80.

[15] R. R. Dayal, R. E. Johnson, A. Muan, Stability of mullite as derived from equilibria in the system CoO-Al_2O_3-SiO_2, J. Am. Ceram. Soc. 50 (2010) 537-540.

[16] H. P. A. Alves, J. B. Silva, L. F. A. Campos, S. M. Torres, R. P. S. Dutra, D. A. Macedo, Preparation of mullite based ceramics from clay-kaolin waste mixtures, Ceram. Int. 42 (2016) 19086-19090.

[17] H. Schneider, J. Schreuer, B. Hildmann, Structure and properties of mullite-A review[J]. J. Eur. Ceram. Soc. 28 (2008) 329-344.

[18] J. Cao, X. Dong, L. Li, Y. Dong, S. Hampshire, Recycling of waste fly ash for production of porous mullite ceramic membrane supports with increased porosity, J. Eur. Ceram. Soc. 34 (2014) 3181-3194.

[19] R. Zhang, C. Ye, X. Hou, S. Li, B. Wang, Microstructure and properties of lightweight fibrous porous mullite ceramics prepared by vacuum squeeze moulding technique, Ceram. Int. 42 (2016) 14843-14848.

[20] A. R. Boccaccini, S. Atiq, D. N. Boccaccini, I. Dlouhy, C. Kaya, Fracture behaviour of mullite fibre reinforced-mullite matrix composites under quasi-static and ballistic impact loading, Compos. Sci. Technol. 65 (2005) 325-333.

[21] Y. Wang, H. Liu, H. Cheng, J. Wang, Densification behavior and microstructure of mullite obtained from diphasic Al_2O_3-SiO_2 gels, Ceram. Int. 40 (2014) 12789-12796.

[22] J. Zhang, H. Wu, S. Zhang, J. Yu, H. Xiao, Anisotropic grain growth in diphasic-gelderived vanadium pentoxide doped mullite, J. Cryst. Growth. 364 (2013) 11-15.

[23] M. H. Ghaemi, S. Reichert, A. Krupa, et al, Zirconia ceramics with additions of alumina for advanced tribological and biomedical applications, Ceram. Int. 2017.

[24] P. Hvizdoš, M. Álvaro, M. Anglada. Effect of heat treatment on wear damage mechanisms in 3Y-TZP ceramics, Wear. 269 (2010) 26-30.

[25] Y. Q. Huang, Z. Li, et al, Effects of the content of in-situ grown mullite on the microstructure and mechanical properties of 3Y-TZP ceramics fabricated by

gel-casting. Ceram. Int. 44 (2018) 21882-21892.

[26] P. F. Liu, Z. Li, et al, Microstructure and mechanical properties of in-situ grown mullite toughened 3Y-TZP zirconia ceramic fabricated by gelcasting, Ceram. Int. 44 (2018) 1394-1403.

[27] C. R. Zhang, R. J. Liu, X. Y. Liu, et al, Numerical simulation and characterization of materials' porosity, pore size, and surface roughness, Optics & Precision Engineering. 2004.

[28] D. J. W. Barrell, M. Priest, The interaction of wear rate and friction with surface roughness for a lubricated sliding contact, Tribology & Interface Engineering. 43 (2003) 807-814.

[29] W. W. Zhu, H. F. Jiang, H. Zhang, Effect of TiO_2 and CaF_2 on the crystallization behavior of Y_2O_3-Al_2O_3-SiO_2 glass ceramics, Ceram. Int. 44 (2018) 6653-6658.

[30] M. L. Mecartney, Influence of an amorphous second phase on the properties of yttria-stabilized tetragonal zirconia polycrystals (Y-TZP), J. Am. Ceram. Soc. 70 (1987) 54-58.

[31] H. Qin, X. Huang, Microstructure and bending strength of 3Y-TZP/12Ce-TZP ceramics fabricated by liquid-phase sintering at low temperature, J. Am. Ceram. Soc. 83 (2000) 2881-2883.

Table and Figure Captions

Table 1. Performance parameters of mated ring and oil used.

Table 2. Experimental parameters of all tribological tests.

Table 3. The mechanical properties of Mullite/3Y-TZP composite ceramics with different content of mullite.

Figure. 1. The picture above is the actual picture of the friction experiment; The picture below is the schematic diagram of the friction experiment.

Figure. 2. XRD patterns of samples with different content of mullite sintered at optimal temperature.

Figure. 3. **(a-c)** represents microscopic topographies of surfaces of different samples (S1,S2 and S5), respectively.

Figure. 4. Morphology and element distribution of the sample containing 4mol% mullite: **(a)** Morphology; **(b)** Zr distribution; **(c)** Al distribution; **(d)** Si distribution; **(e)** Y distribution; **(f)** O distribution.

Figure. 5. The coefficient of friction of different samples (S1-S5) after rubbing in an oily environment.

Figure. 6. The wear rate of different samples (S1-S5) after rubbing in an oily environment.

Figure. 7. 3D microscopic topography of the worn surface of different samples (S1-S5).

Figure. 8. The morphology of worn surface of different samples after rubbing in an oily environment (S1-S5).

Figure. 9. Further enlargement of the worn surfaces of different samples (S1,S2,S5).

Figure. 10. Schematic diagram of different wear mechanisms that may occur during the experiment.

Table 1. Performance parameters of mated ring and oil used

	Chemical composition of Cr_{26}				Hardness（HRC）
Mated ring（Cr_{26}）(wt%)	Cr	Si	Mn	S	≥56
	26	≤0.8	0.8-1	≤0.06	
	C	P	Ni	Cu	
	2.7-2.9	≤0.15	0.5-1.5	≤2.0	
	Viscosity		Function		
Engine oil	15W-40		Protection and maintenance		

Table 2. Experimental parameters of all tribological tests

Content of mullite (mol%)	Tribological parameters				
	Rotating speed (r/min)	Loading (N)	Time (min)	Temperature (℃)	Lubricant
2	200	150	30	28	engine oil
4					
6					
8					
10					

Table 3. The mechanical properties of Mullite/3Y-TZP composite ceramics with different content of mullite.

Content of mullite (mol%)	Mechanical parameters of different samples (average results from 5 tests)			
	Open porosity (%)	Flexural strength (MPa)	Fracture toughness K_{IC} ($MPa \cdot m^{1/2}$)	Vickers hardness HV (GPa)
2	0.2	785.81	10.04	13.10
4	0.15	907.31	10.38	13.02
6	0.24	633.59	7.76	12.07
8	0.31	517.97	5.72	11.32
10	0.36	502.85	4.67	10.67

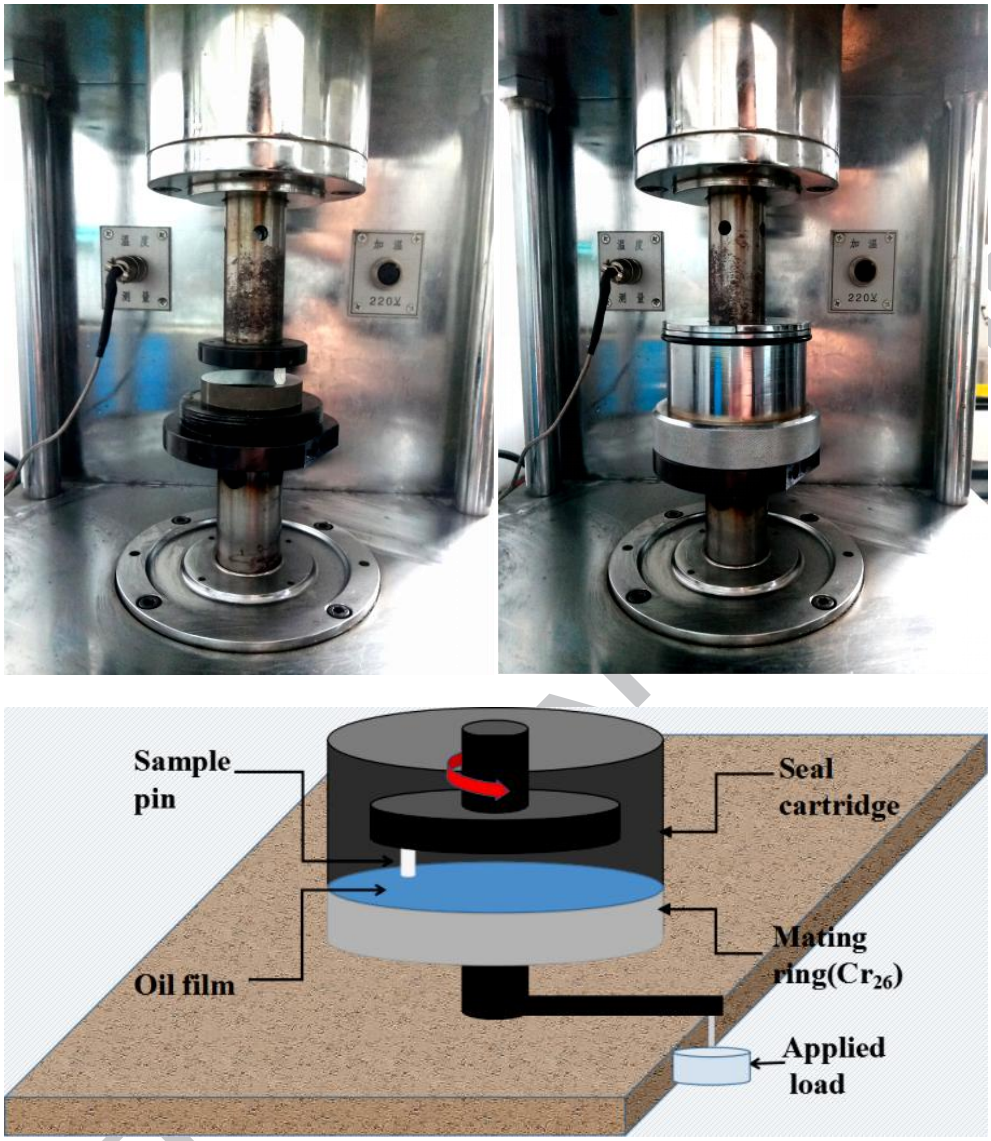

Figure. 1. The picture above is the actual picture of the friction experiment; The picture below is the schematic diagram of the friction experiment

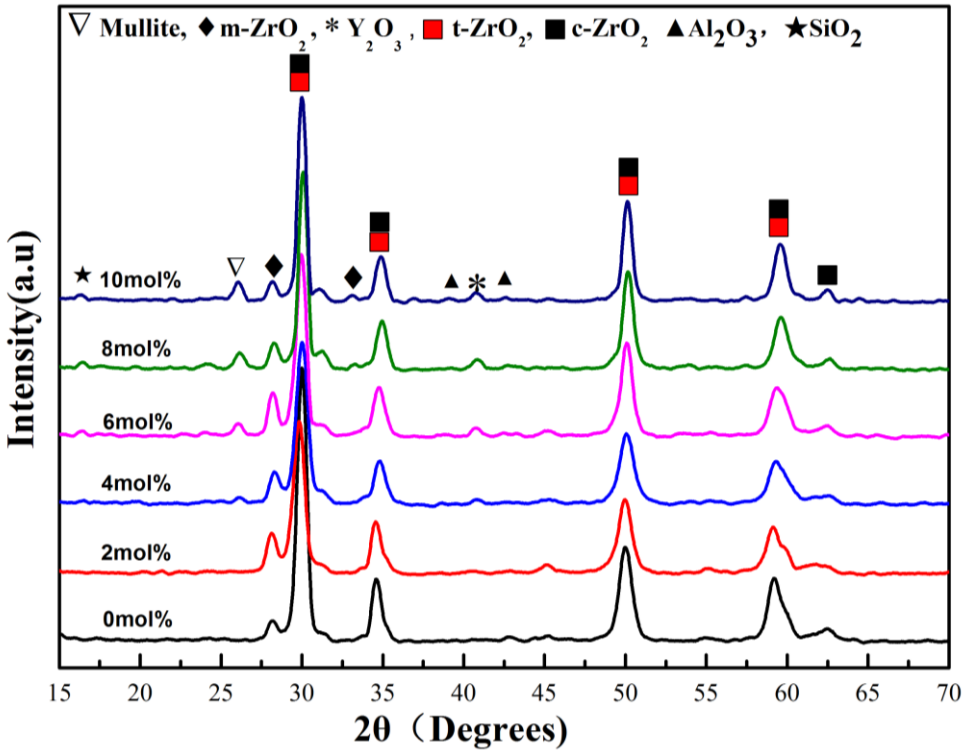

Figure. 2. XRD patterns of samples with different content of mullite sintered at optimal temperature.

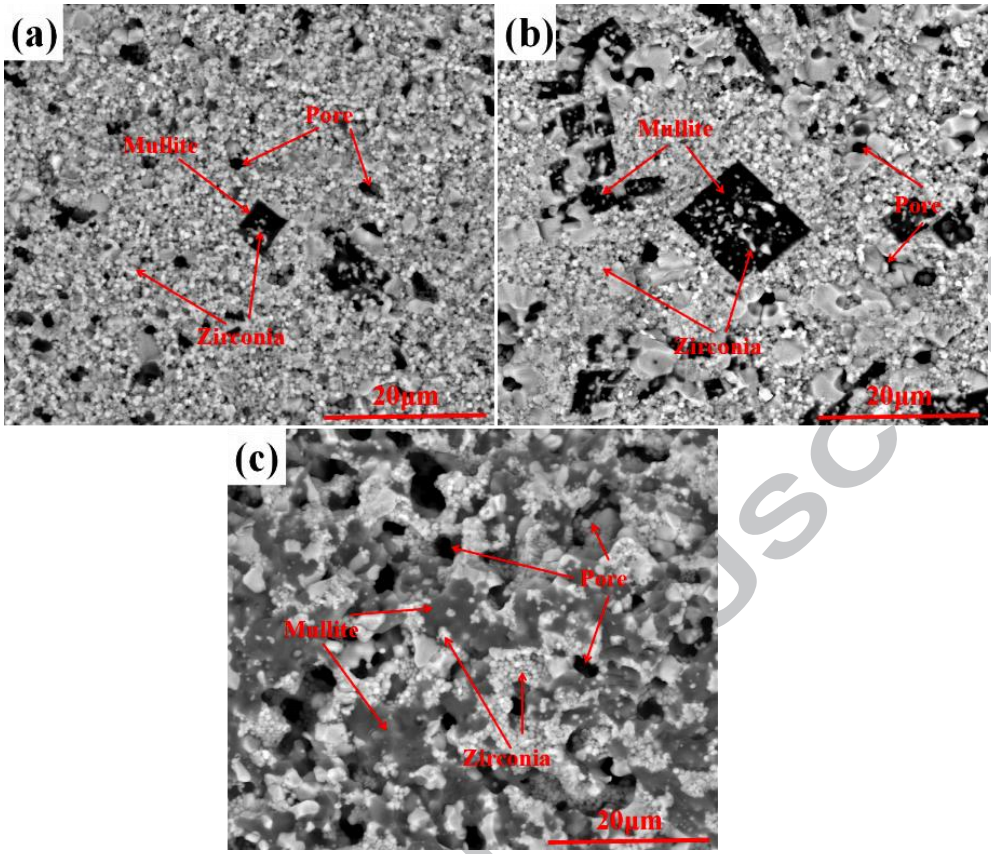

Figure. 3. (a-c) represents microscopic topographies of surfaces of different samples (S1,S2 and S5), respectively.

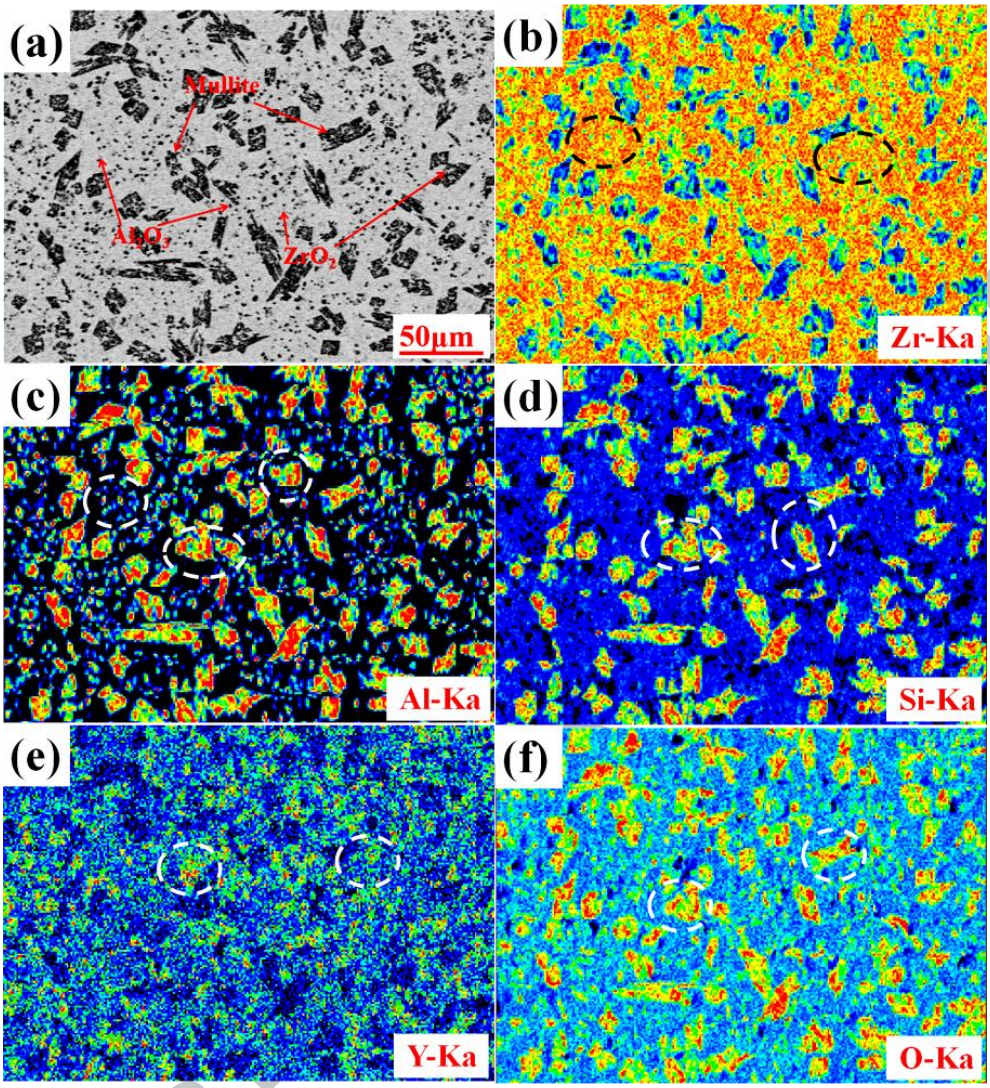

Figure. 4. Morphology and element distribution of the sample containing 4mol% mullite: **(a)** Morphology; **(b)** Zr distribution; **(c)** Al distribution; **(d)** Si distribution; **(e)** Y distribution; **(f)** O distribution.

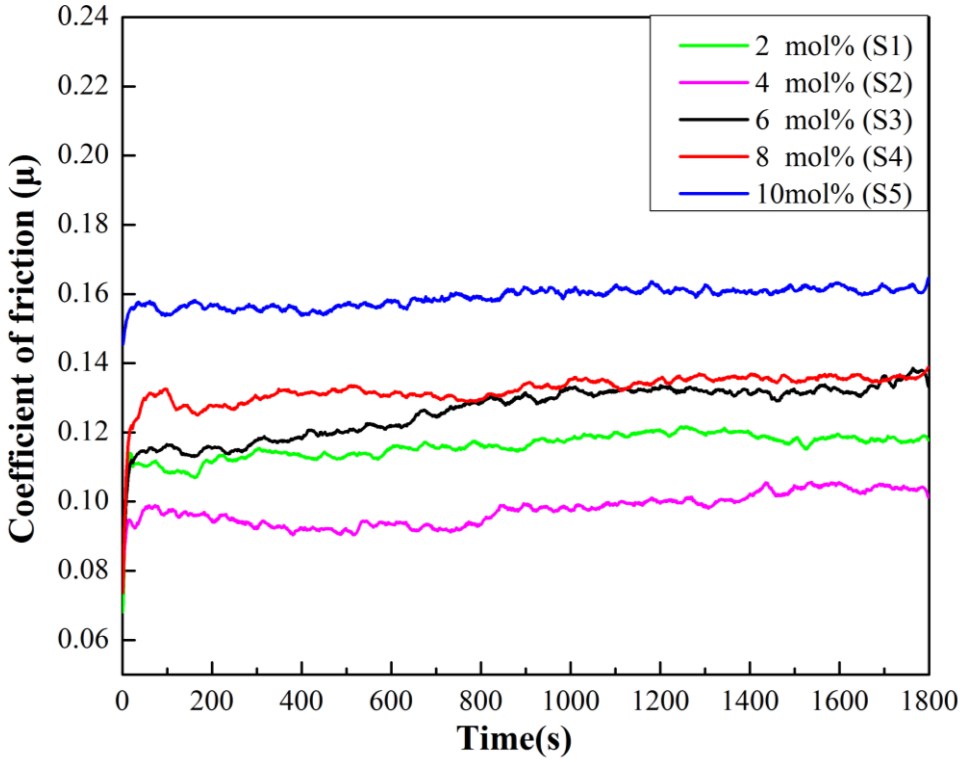

Figure. 5. The coefficient of friction of different samples (S1-S5) after rubbing in an oily environment.

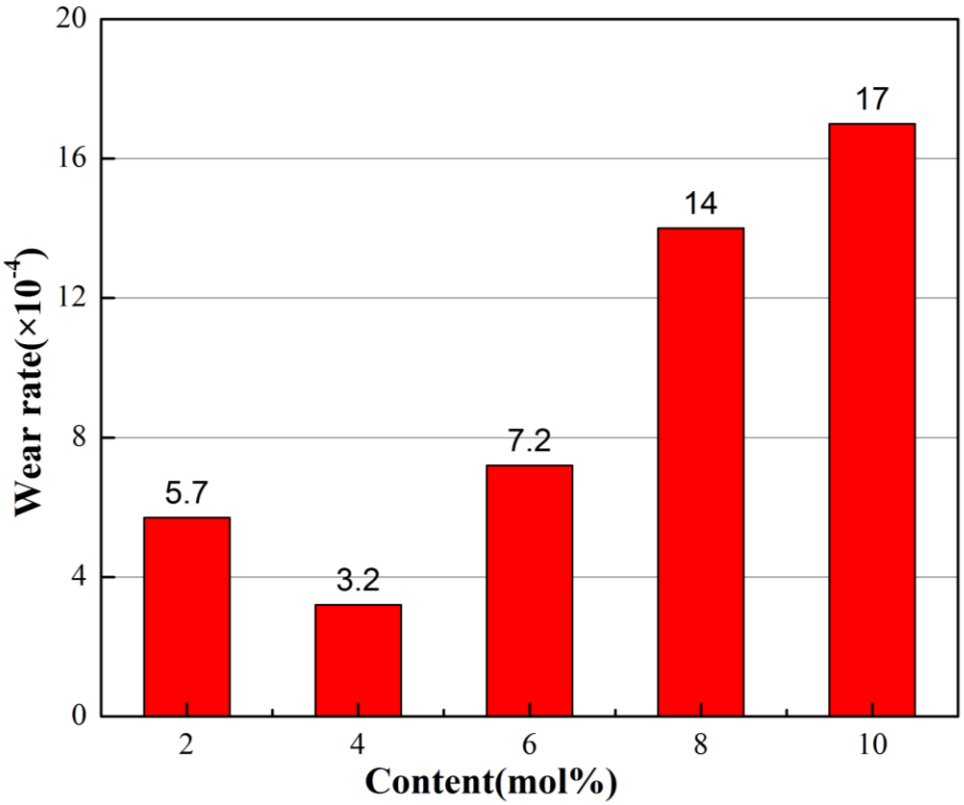

Figure. 6. The wear rate of different samples (S1-S5) after rubbing in an oily environment.

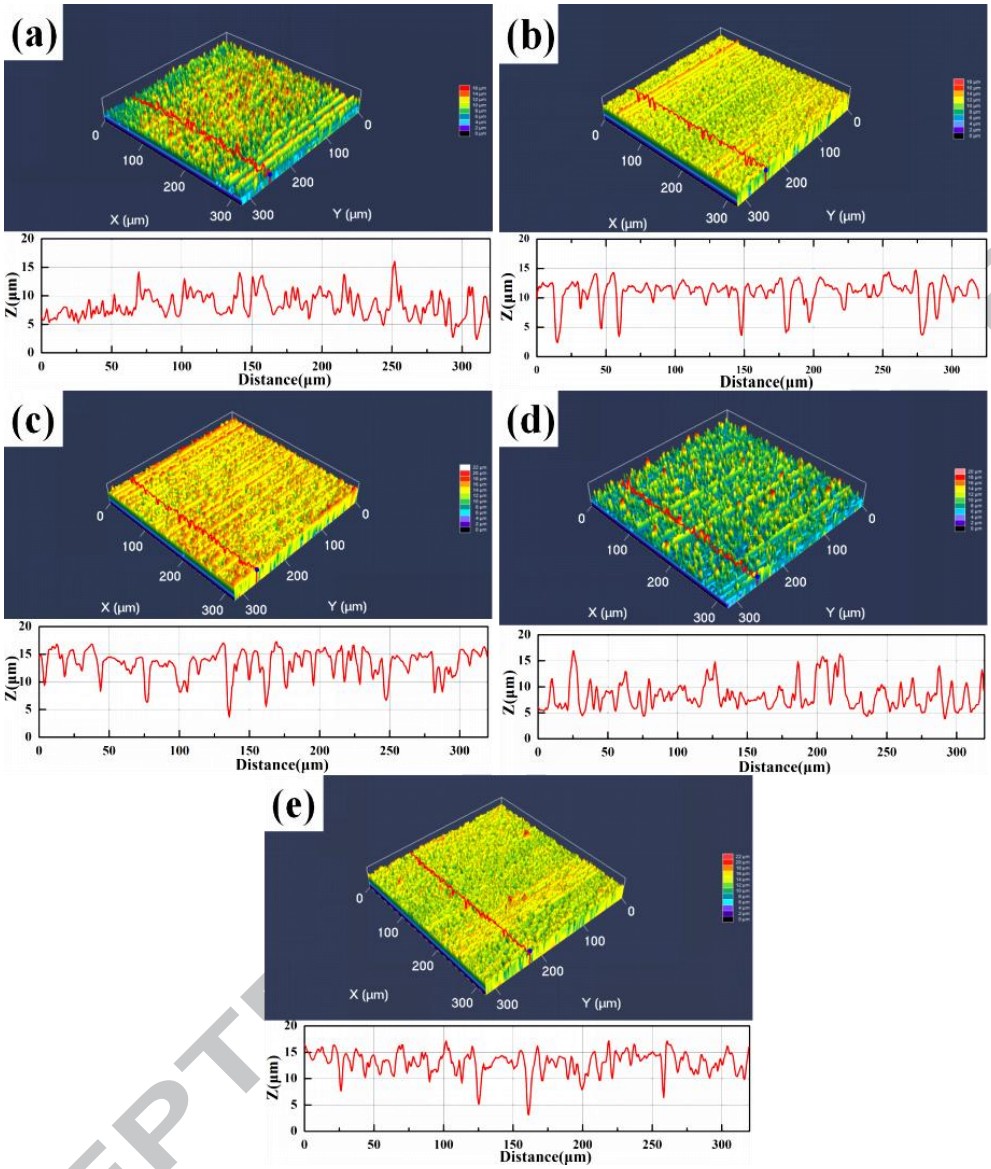

Figure 7. 3D microscopic topography of the worn surface of different samples (S1-S5).

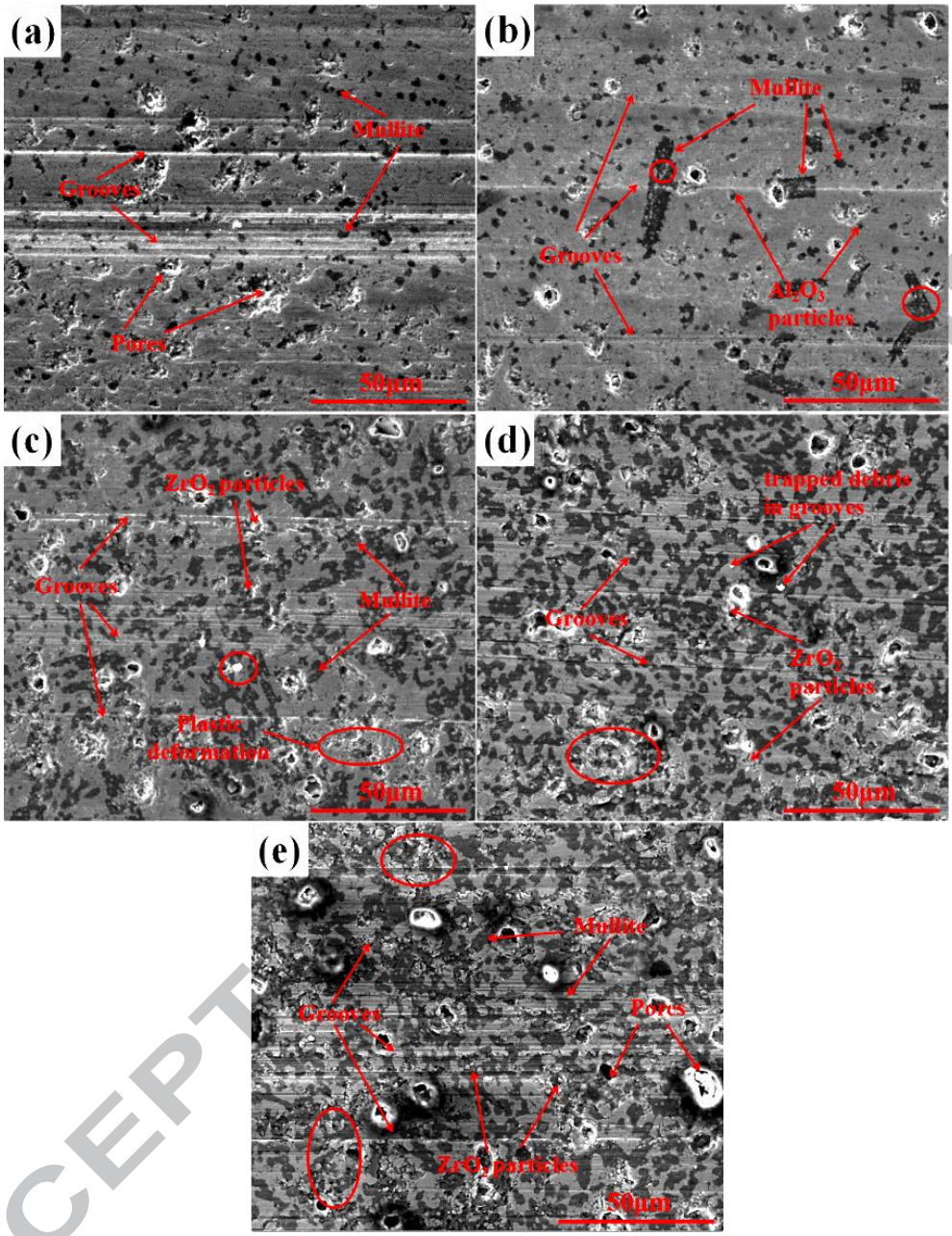

Figure. 8. The morphology of worn surface of different samples after rubbing in an oily environment (S1-S5).

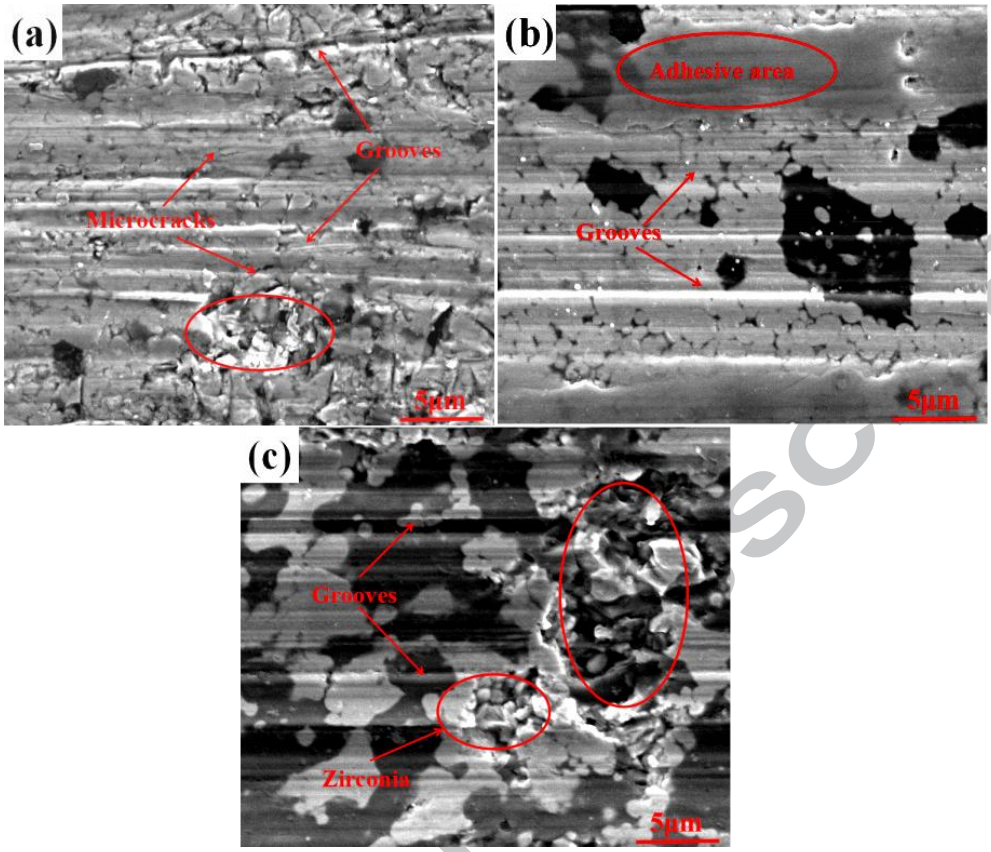

Figure 9. Further enlargement of the worn surfaces of different samples (S1,S2,S5).

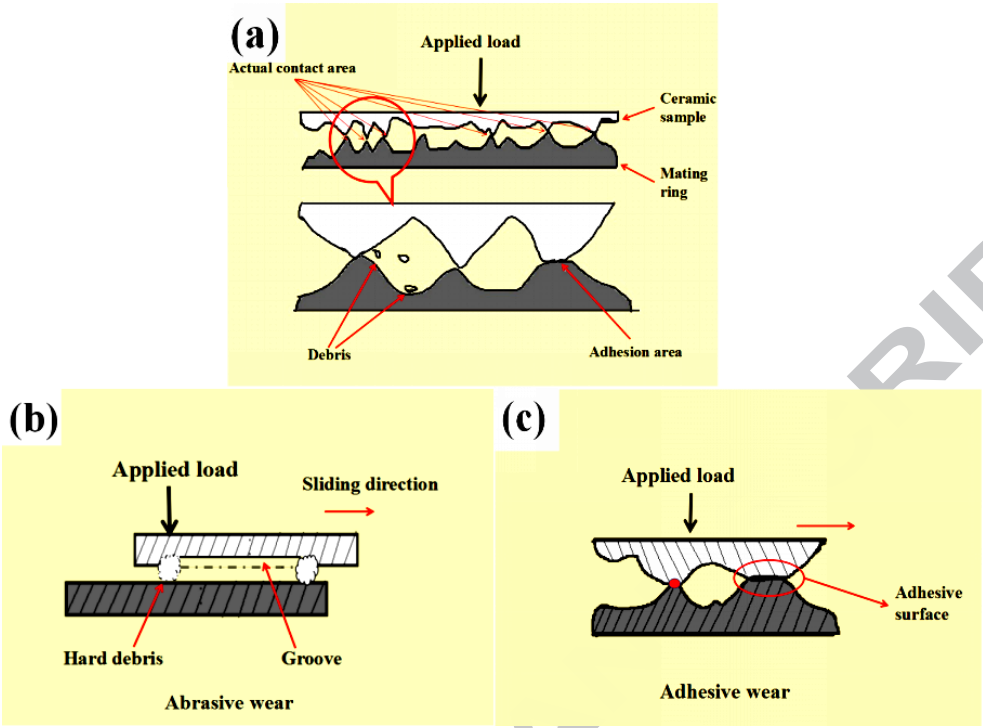

Figure 10. Schematic diagram of different wear mechanisms that may occur during the experiment.

Highlights

The effect of the content of mullite on the microstructure and tribological properties of Mullite/3Y-TZP composite ceramics was investigated in depth. A theoretical model of wear mechanism was established based on the wear surface morphology, revealing the wear mechanism of Mullite/3Y-TZP composite ceramics.